SINTECHCOM: Science, Technology and Communication Journal
Vol. 5, No. 3, June 2025, pp. 91-100, DOI: 10.59190/stc.v5i3.307

Green-synthesized ZnO and Ag nanoparticles: A comparative study of optical, morphology and structural properties for photocatalytic applications

Yanuar Hamzah*, Tengku Emrinaldi, Rahmi Dewi, Ari Sulistyo Rini, Lazuardi Umar, Mediniah Putri Simatupang, Rabiah, Muhammad Deri Noferdi
Department of Physics, Universitas Riau, Pekanbaru 28293, Indonesia

ABSTRACT

In this study, zinc oxide (ZnO) and silver (Ag) nanoparticles were synthesized using *Annona muricata* leaf extract as a reducing and stabilizing agent with variations in the molar ratio of 1:3, 1:5, and 1:7. Optical characterization using UV-Visible spectroscopy revealed that the variations of molar ratio influence the absorption peak and band gap energy of the resulting ZnO and Ag. UV-Vis results show that the molar ratio 1:5 was optimal for synthesizing ZnO and Ag. The band gap value of synthesized ZnO and Ag at a 1:5 molar ratio was 3.27 eV and 2.01 eV, with absorption peaks at 355 nm and 435 nm respectively. XRD characterization shows that ZnO nanoparticles has a hexagonal wurtzite structure with lattice parameters of a = 76 Å and c = 4. 95 Å and for Ag nanoparticles has a face centered cubic structure with lattice parameters $a = b = c$ is 4.15 Å. *Annona muricata* leaves extract shows photocatalytic properties that can be applied to the degradation of polluted water. This shows that ZnO nanoparticles via green synthesis using *Annona muricata* leaf extract is a very simple, low-cost and environmentally friendly method.

ARTICLE INFO

Article history:

Received Apr 20, 2025
Revised May 22, 2025
Accepted Jun 23, 2025

Keywords:

Annona muricata
Nanoparticles
Photocatalytic
Silver
Zinc Oxide

* **Corresponding Author**
E-mail address: yanuar.hamzah@lecturer.unri.ac.id

1. INTRODUCTION

Water pollution is a major global environmental issue that must be addressed. Industrial processes, in most cases, produce waste materials that are toxic and persistent. These wastes are often directly discarded into water bodies and give rise to grievous environmental pollution [1]. Among various pollutants, dyes such as methylene blue (MB) are one of the major contaminants extensively used as colorants in textiles, paper, and plastics [2]. MB has a poor degradation efficiency under natural processes, and its presence in water bodies might pose a risk to aquatic life and human health. Long-term exposure to MB might cause health issues such as nausea, vomiting, headache, eye irritation, vertigo, and stomach upset [3]. Therefore, it is crucial to remove MB from the water body efficiently.

Methods including adsorption [4], filtration [5, 6], ion exchange [7], and advanced oxidation [8], are commonly used to remove MB from the environment. However, these methods are expensive, have low efficiency at removing pollutants, and produce hazardous intermediate chemicals [9]. Among the various techniques, photocatalysis is considered promising because of its low operating costs, simple technique, accessibility, and exceptional performance [10]. The photocatalysis method is a type of advanced oxidation process (AOP) that transforms colored compounds into colorless reductive metabolites. To improve the degradation of dyes, a catalyst is used in this process to help produce high-reactive radicals [11]. In the photocatalysis process, light is used to initiate and accelerate chemical reactions. Because of this, metal nanoparticles that have a characteristic property

of light absorption attracted considerable attention [12]. ZnO and Ag nanoparticles have become particularly attractive for photocatalytic applications.

ZnO is a semiconductor metal, its photocatalytic activity is associated with the absorption of light and the generation of electron/hole pairs. These electron/hole pairs could participate in photocatalytic reactions that degrade organic pollutants and eliminate dangerous substances [13]. Meanwhile, Ag nanoparticles received attention because of their surface plasmon resonance (strong absorption in the visible region), which can be easily monitored using a UV–visible spectrophotometer [14]. The electrons on the surface of Ag nanoparticles can be excited by UV or visible light, which can contribute to photocatalytic reactions and produce free radicals [15].

Biosynthesis offers an eco-friendly and sustainable alternative to conventional nanoparticle synthesis methods. Plants have great potential for detoxifying heavy metals and other harmful substances and are recognized as cost-effective producers of natural chemical compounds [16]. Because of its natural reducing and stabilizing agents, plant extracts eliminate the need for hazardous chemicals and energy-intensive processes to synthesize various nanoparticles [17]. Previous studies have employed plant extracts such as *Lentinula edodes* [18], *Cocos nucifera* [19], *Areca catechu* [20], and *Citrullus colocynthis* [21] to biosynthesize nanoparticles. In this present study, zinc and silver nanoparticles were biosynthesized using *Annona muricata* leaf extract were investigated. The synthesized nanoparticles are characterized using UV-Vis spectroscopy and x-ray diffraction (XRD) to determine their optical and structural properties. Additionally, their photocatalytic performance is evaluated in the degradation of MB under visible light, to demonstrate their potential for environmental remediation.

2. RESEARCH METHODS

The synthesis of ZnO and Ag nanoparticles began with the preparation of *Annona muricata* leaf extract. The leaves were thoroughly washed and dried in a microwave at 100°C for 120 minutes to remove moisture and impurities. The dried leaves were ground and sieved to obtain a fine powder. 5 g of the leaf powder was dissolved in 200 mL of distilled water and heated to 80°C for 10 minutes with continuous stirring using a magnetic stirrer. The solution was then cooled to room temperature and filtered using Whatman No. 1 filter paper. The resulting filtrate served as the *Annona muricata* leaf extract, which was used as a bio-reductant in the ZnO and Ag nanoparticle synthesis.

ZnO nanoparticles were synthesized by reacting 0.5 M zinc nitrate ($Zn(NO_3)_2$) solution with *Annona muricata* leaf extract in molar ratios of 1:3, 1:5, and 1:7. To adjust the pH to 7, several drops of 1 M NaOH solution were added. The mixture was heated to 80°C for 1 hour, producing a white precipitate. This precipitation was separated using a centrifuge at 4000 rpm for 10 minutes and then dried on a hot plate at 125°C.

Silver nanoparticles were synthesized by reacting 0.01 M silver nitrate ($AgNO_3$) solution with *Annona muricata* leaf extract (50 g/L) as a reducing agent in volume ratios of 1:1, 1:3, and 1:7. The reaction was carried out in the presence of NaOH at pH 7 as a stabilizing agent. Optical properties were characterized using an Agilent Cary 60 UV-Vis spectrophotometer in the 200 to 700 nm range. The crystal structure was analyzed by XRD with a X'Pert PRO PANalitycal MPD PW3040/60 Diffractometer and $\lambda CuK\alpha = 1.541$ Å.

MB solution was diluted from 25 to 5 ppm using distilled water in a 50 mL volumetric flask. That 5 ppm solution was analyzed with a UV-Vis spectrophotometer to determine its maximum absorption wavelength. The degradation test was performed by adding 0.1 g of Ag or ZnO nanoparticle powder into 25 mL of the MB solution in a beaker. The mixture was stirred with a magnetic stirrer for uniform dispersion and irradiated under UV light at varying times. After 150 minutes, the solution was filtered, and 3 mL of the filtrate was analyzed for absorbance using a UV-Vis spectrophotometer to evaluate the degradation efficiency. The sample analyzed for XRD characterization and MB degradation testing was selected based on its optimal absorbance properties identified through UV-Vis spectroscopy.

3. RESULTS AND DISCUSSIONS

The synthesis of ZnO and Ag using *Annona muricata* leaf extract was conducted with variations in the molar ratio of extract to ZnO and zinc nitrate precursor, specifically 1:3, 1:5, and 1:7,

to evaluate its impact on the material optical properties, as shown in Figure 1. From UV-Visible spectroscopy analysis, each molar variation showed changes in the primary absorption wavelength of ZnO, which correlates with the band gap energy of the material. At a molar ratio 1:3, the absorption peak appeared at around 365 nm, yielding a band gap energy of 3.30 eV.

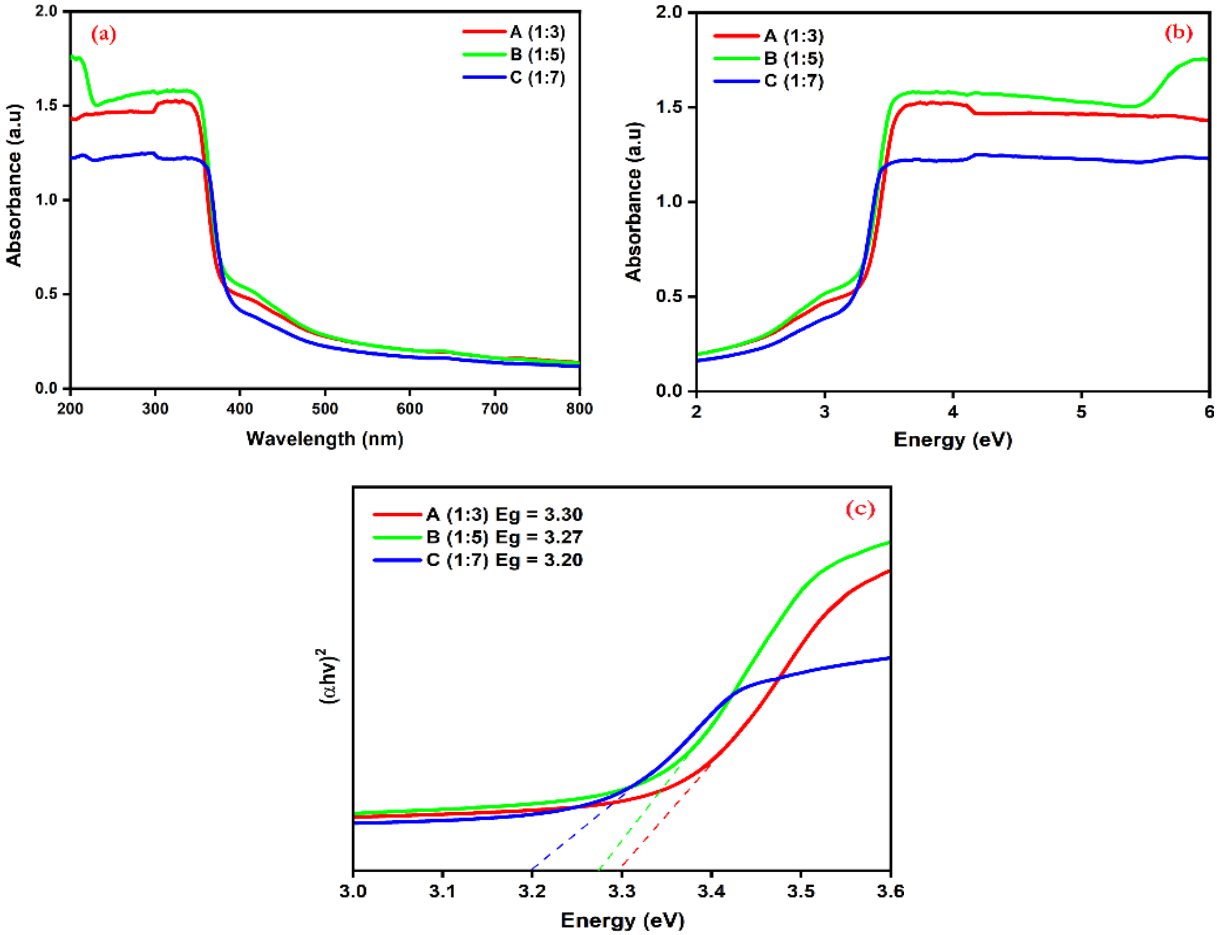

Figure 1. UV-Vis spectroscopy analysis of ZnO nanoparticles (a) Absorbance spectra (b) Relation between absorbance vs energy (c) Band gap energy curves with variations in the molar ratio of extract to Zinc precursor of sample (1:3), (1:5), and (1:7).

This value indicates a redshift (shift to a higher wavelength) compared to the typical band gap value for pure ZnO of around 3.2 eV [22]. This shift suggests that a lower concentration of *Annona muricata* leaf extract produces slightly larger ZnO particle sizes or weaker interactions with the bioactive compounds in the extract, which may reduce the band gap energy of ZnO [23]. Furthermore, at a molar ratio 1:5, the absorption peak shifted to a wavelength of 355 nm, with a band gap energy of 3.27 eV. This shift to a shorter wavelength is known as a blue shift, indicating that an increase in extract concentration causes the ZnO particle size to decrease or strengthen the interaction between ZnO particles and bioactive compounds in the extract [24]. This could be attributed to the role of bioactive components in the extract, such as phenolics and flavonoids, which stabilize ZnO nanoparticles, resulting in a slightly wider band gap energy [25].

At the highest molar ratio of 1:7, the ZnO absorption peak exhibited a further blue shift to 350 nm, with a band gap energy of 3.20 eV. This additional shift suggests that the higher extract concentration provides more bioactive compounds interacting with the ZnO surface, enhancing the stabilizing effect and resulting in smaller particle sizes or a more modified electronic structure [26].

The analysis of Ag from UV-Vis spectroscopy (Figure 2) also shows changes in primary absorption wavelength with each molar ratio variation. At a molar ratio 1:3, the absorption peak appeared at around 439 nm, with a band gap energy of 1.84 eV. At 1:5 and 1:7 molar ratios, Ag shows

an absorption peak at 435 nm and 425 nm, with the band gap energy respectively at 2.01 eV and 2.04 eV. The results of absorption peak below 500 nm confirm the successful formation of silver nanoparticles [27, 28]. The shift to a shorter wavelength at a higher molar ratio of *Annona muricata* leaf extract indicates that the average particle size of synthesized Ag produced was decreasing because of the biocomponent in the extract that interacts with $AgNO_3$. The band gap energy increases with a decrease in the size of the nanoparticles causing an overlapping number of orbitals or decreasing band energy. This condition causes an increase in separations between the valence band and conduction, because of this greater separation the energy band gap also increases [29].

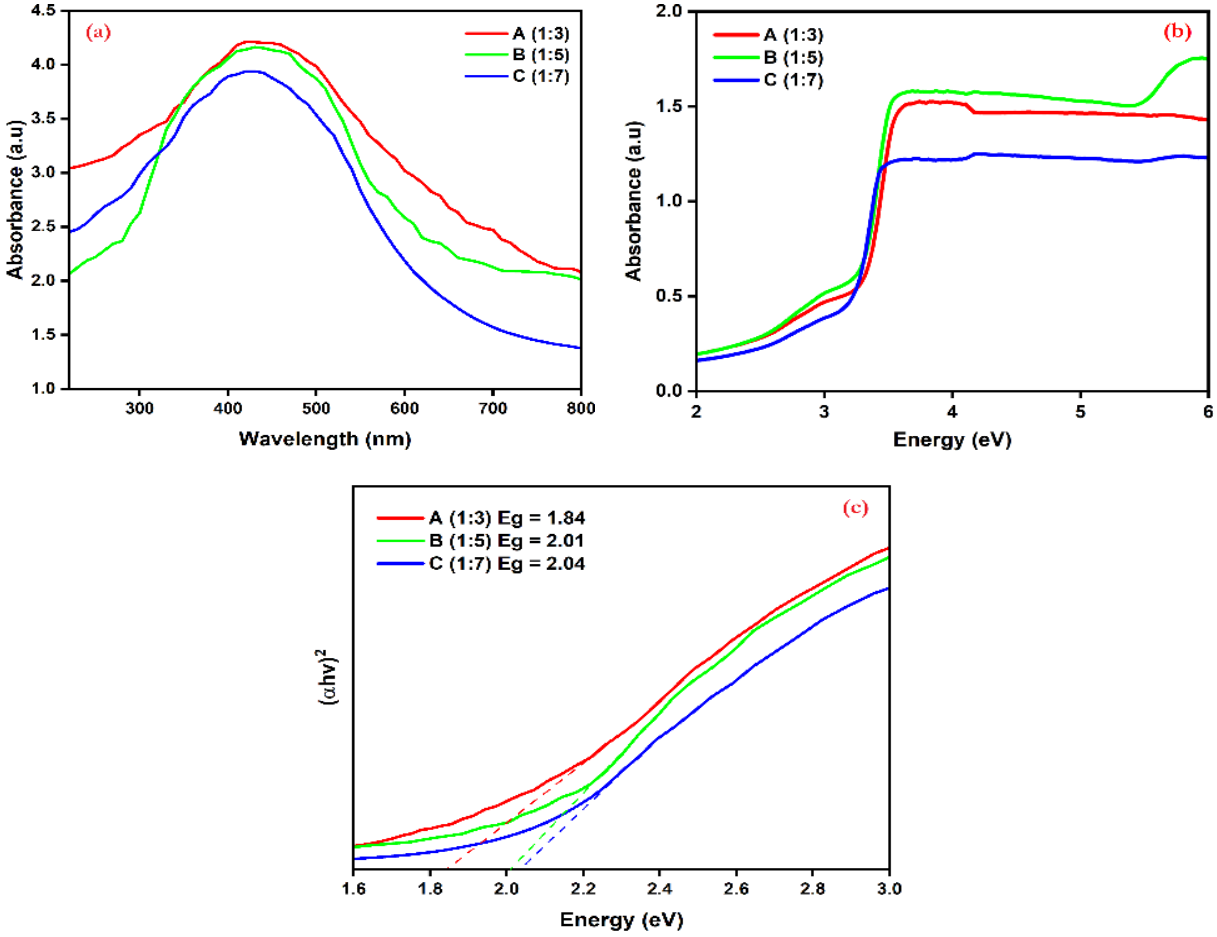

Figure 2. UV-Vis spectroscopy analysis of Ag nanoparticles (a) absorbance spectra (b) relation between absorbance vs energy (c) band gap energy curves with variations in the molar ratio of extract to silver precursor of sample (1:3), (1:5), and (1:7).

The Tauc method was used to analyze the band gap energy of ZnO and Ag. This method involves plotting $(\alpha hv)^2$ versus hv, where α is the absorption coefficient, h is Planck's constant, and v is the frequency of light. The value of n is 2, indicating a direct band gap. The band gap energy Eg is obtained by drawing a straight line along the linear part of the plot and extending it to intercept the x- axis. The intercept on the x - axis (where $(\alpha hv)^2 = 0$) gives the Eg value. The formula is provided in Equation (1), and the curve is shown in Figure 1 and Figure 2.

$$(\alpha hv)^2 = A(hv - Eg) \quad (1)$$

Overall, these results indicate that increasing the molar ratio of *Annona muricata* leaf extract not only affects the size and stability of ZnO and Ag particles but also causes blue or red shifts in the UV-Vis spectrum, reflecting changes in the band gap energy. This effect underscores the role of

Annona muricata leaf extract not only as a reducing agent but also as a tailor of the optical properties of the synthesized ZnO and Ag [30].

XRD characterization aims to determine the phase in the sample. XRD patterns are analyzed on the *hkl* plane of a crystal. Differences in crystal plane orientation cause patterns to appear in the form of different peaks at certain diffraction angles. Bragg's law can estimate the diffraction that occurs in an atomic crystal.

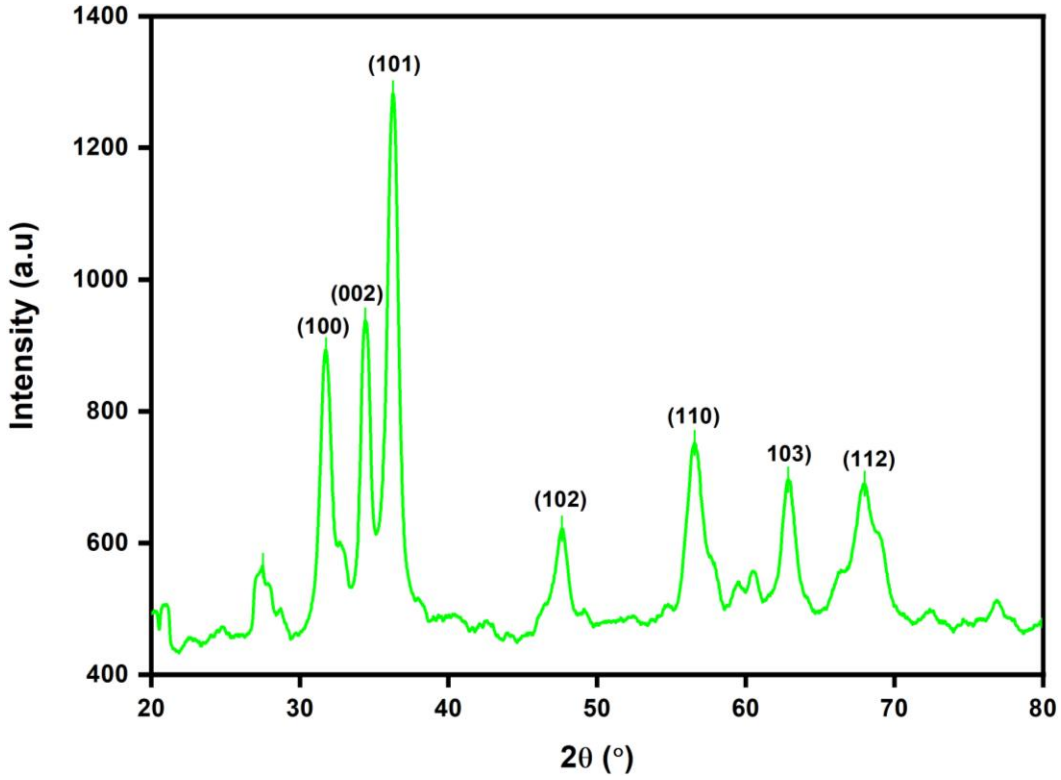

Figure 3. XRD pattern of ZnO nanoparticle sample 1:5.

Figure 3 shows the XRD pattern on the ZnO 1:5 sample. In the diffraction pattern, diffraction peaks can be seen at an angle of 2θ, the results of the XRD that has been carried out are formed at an angle 31.74°, 34.37°, 36.24°, 47.60°, 56.55°, 62.84°, and 67.99° with *hkl* planes respectively (100), (002), (101), (102), (110), (103), and (112) [31]. Figure 3 confirms that the sample shows ZnO growth orientation with the highest peak at a diffraction angle of 2θ around 36 *hkl* plane (101). Figure 3 confirms that the sample shows the ZnO growth orientation with the highest peak at the diffraction angle of 2θ around 36 *hkl* plane (101). Based on the JCPDS No. 36-1451 database, ZnO has a hexagonal crystal system with lattice parameter values of $a = b = 2.76$ Å and $c = 4.95$ Å.

Figure 4 shows the XRD pattern on the Ag nanoparticle 1:5 sample. In the diffraction pattern, diffraction peaks can be seen at an angle of 2θ from the XRD results that have been carried out, namely at angles 28.5°, 37.52°, 42.32°, 63.92°, and 76.8° with the *hkl* planes respectively (101), (111), (200), (202), and (311). Then, the results obtained were compared with the Joint Committee on Powder Diffraction Standard (JCPDS) No. 04-0783 database. For Ag nanoparticles, they have an FCC crystal system with lattice parameter values of $a = b = c = 4.15$ Å. The crystallite size of the Ag and ZnO sample was calculated based on the X-ray diffraction pattern broadening data using the Scherrer equation given by Equation (2) [32].

$$D = \frac{K\lambda}{\beta \cos\theta} \quad (1)$$

where, D is the crystallite size, K is the Scherrer constant of 0.90, λ is the X-ray wavelength (for the CuKα source it is 1.5418 Å), β is the full width at half maximum (FWHM) of the XRD pattern peak,

and θ is the diffraction angle [33]. The calculation results obtained the average crystallite size of the ZnO and Ag samples. The average crystallite size of the ZnO sample (1:5) is 59.68 nm, which is larger compared to the Ag nanoparticle sample (1:5) which is 35.31 nm.

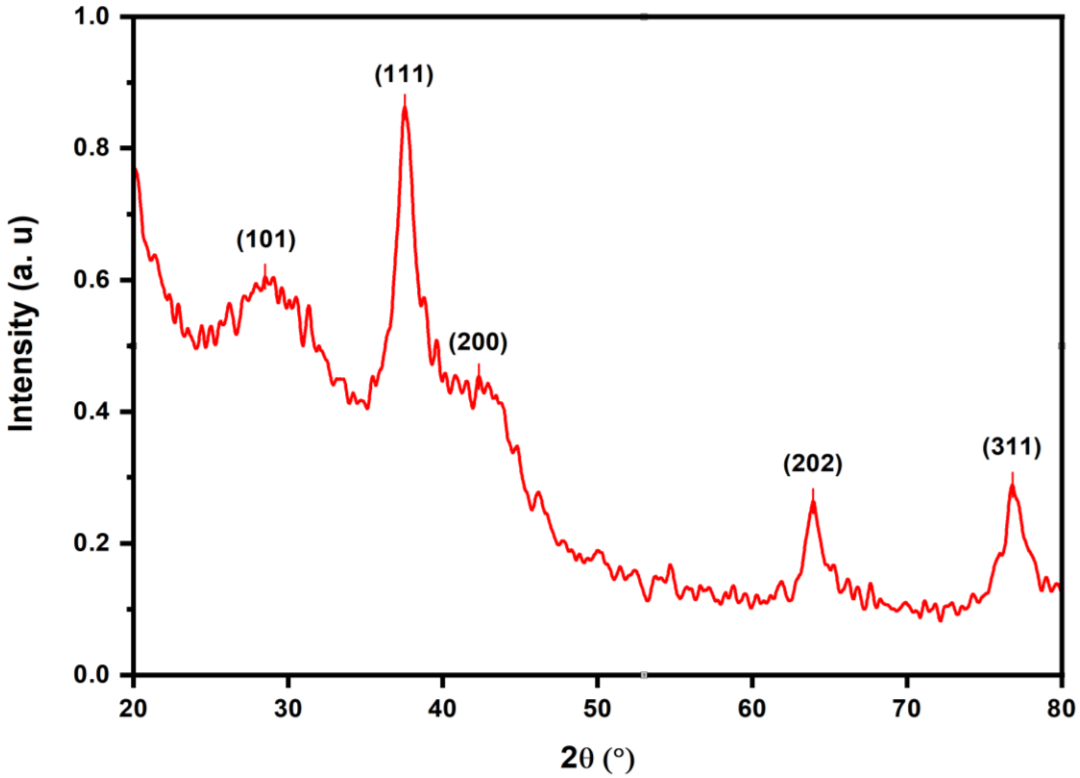

Figure 4. XRD pattern of Ag nanoparticle sample 1:5.

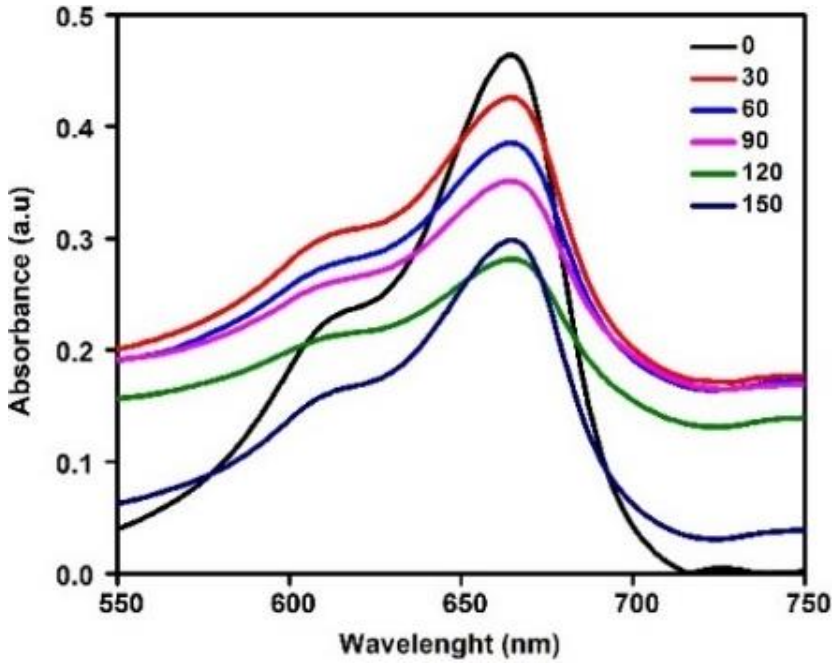

Figure 5. The degradation of MB ZnO nanoparticles sample (1:5).

The photocatalysis results using ZnO and Ag as catalysts for MB degradation over 150 minutes with UV light showed a decrease in absorbance intensity in the UV-Vis spectrum graph

(Figure 5 and Figure 6). The degradation percentage of MB by ZnO reached 79.91% with a reaction rate of -0.00354 min^{-1}, while Ag achieved a degradation percentage of 79.38% with a reaction rate -0.00351 min^{-1}.

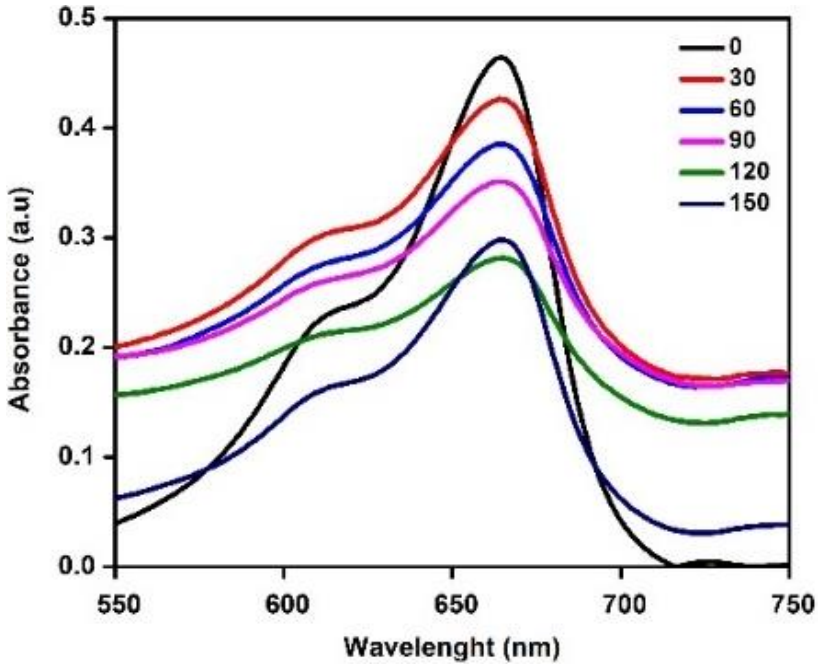

Figure 6. The degradation of MB Ag nanoparticles sample (1:5).

The observed shift in the UV-Vis spectrum curve, either a redshift or blueshift, and the appearance of additional peaks can be attributed to several factors. The shift in the primary absorbance peak is commonly caused by the partial degradation of the MB structure, leading to the formation of intermediate products with different optical properties. These are formations of intermediate products with different optical properties. These intermediates absorb light at different wavelengths, resulting in the appearance of new peaks or shifts in the absorbance spectrum [34].

Moreover, the photocatalytic activity generates reactive species such as hydroxyl radicals (*OH*) and superoxide ions O_2^-, which progressively break down the aromatic structure of MB [31]. As the degradation proceeds, intermediate degradation products may still possess absorbance capabilities within the measured UV-Vis range, thus explaining the emergence of additional peaks with lower intensity. This phenomenon can also be influenced by the photocatalytic mechanism, which involves complex interactions between photons, excited electrons in the conduction band, and holes in the valence band [35]. These interactions contribute to the degradation of MB molecules and the formation of temporary by products, resulting in the observed spectral shifts and peak variations. Future research should focus on investigating the morphological properties and FTIR spectroscopy to identify functional groups exhibits distinct properties [36].

4. CONCLUSIONS

Annona muricata leaf extract can act as a reducing agent for zinc nitrate and silver nitrate solutions to produce ZnO and Ag nanoparticles. UV-vis absorption analysis showed absorbance with a range of 300 to 400 nanometers for ZnO nanoparticles and for Ag nanoparticles in a wavelength range of 350 to 450 nm. The energy gap of ZnO nanoparticles and Ag nanoparticles with a ratio of *Annona muricata* leaf extract to zinc and silver nitrate precursors of 1:5 was 3.27 eV and 2.01 eV, respectively. XRD characterization shows that ZnO nanoparticles have a hexagonal wurtzite structure with lattice parameters of $a = b = 2.76$ Å and $c = 4.95$ Å. For nanoparticles have a face centered cubic structure with lattice parameters $a = b = c = 4.15$ Å. The degradation of MB by ZnO reached 79.91%, while Ag was 79.38% at 150 minutes of degradation time. Research on the potential of annona leaves as a

bioreductor for synthesizing ZnO nanoparticles in biomedical applications such as antibacterial needs to be investigated for the future.

ACKNOWLEDGMENTS

The authors would like to thank Faculty of Mathematics and Natural Sciences, Universitas Riau, Pekanbaru, Indonesia for support this research under Research Grants DIPA FMIPA 2023, contract number: 1190r/UN19.5.1.1.3/PL.01.00/202.

REFERENCES

[1] Mishra, R. K., Mentha, S. S., Misra, Y., & Dwivedi, N. (2023). Emerging pollutants of severe environmental concern in water and wastewater: A comprehensive review on current developments and future research. *Water-Energy Nexus*, **6**, 74–95.

[2] Oladoye, P. O., Ajiboye, T. O., Omotola, E. O., & Oyewola, O. J. (2022). Methylene blue dye: Toxicity and potential elimination technology from wastewater. *Results in Engineering*, **16**, 100678.

[3] Fito, J., Abewaa, M., Mengistu, A., Angassa, K., Ambaye, A. D., Moyo, W., & Nkambule, T. (2023). Adsorption of methylene blue from textile industrial wastewater using activated carbon developed from Rumex abyssinicus plant. *Scientific Reports*, **13**(1), 5427.

[4] Ramutshatsha-Makhwedzha, D., Mavhungu, A., Moropeng, M. L., & Mbaya, R. (2022). Activated carbon derived from waste orange and lemon peels for the adsorption of methyl orange and methylene blue dyes from wastewater. *Heliyon*, **8**(8).

[5] Shao, X., Wang, J., Liu, Z., Hu, N., Liu, M., Duan, C., Zhang, R., & Quan, C. (2021). Cellulose based cation-exchange fiber as filtration material for the rapid removal of methylene blue from wastewater. *Cellulose*, **28**, 9355–9367.

[6] Krobthong, S., Rungsawang, T., & Wongrerkdee, S. (2023). Comparison of ZnO nanoparticles prepared by precipitation and combustion for UV and sunlight-driven photocatalytic degradation of methylene blue. *Toxics*, **11**(3), 266.

[7] Liu, H., Yu, J., & Liu, X. (2023). Study on the ozonation degradation of methylene blue enhanced by microchannel and ultrasound. *Water Science & Technology*, **87**(3), 598–613.

[8] Tamizharasan, S., Muralidharan, R., Abirami, N., Leelavathi, H., Siva, A., Kumarasamy, A., & Arulmozhi, R. (2023). Biomass derived carbon blended ion-exchange resins for the removal of toxic metal ions from waste water. *Optik*, **283**, 170930.

[9] Thakur, A. K., Kumar, R., Kumar, A., Shankar, R., Khan, N. A., Gupta, K. N., ... & Arya, R. K. (2023). Pharmaceutical waste-water treatment via advanced oxidation based integrated processes: An engineering and economic perspective. *Journal of Water Process Engineering*, **54**, 103977.

[10] Bharath, G., Banat, F., & Haija, M. A. (2023). Photoelectrochemical advanced oxidation processes for simultaneous removal of antibiotics and heavy metal ions in wastewater using 2D-on-2D WS2@ CoFe2O4 heteronanostructures. *Environmental Pollution*, **339**, 122753.

[11] Ahmed, M., Mavukkandy, M. O., Giwa, A., Elektorowicz, M., Katsou, E., Khelifi, O., Naddeo, V., & Hasan, S. W. (2022). Recent developments in hazardous pollutants removal from wastewater and water reuse within a circular economy. *NPJ Clean Water*, **5**(1), 1–25.

[12] Chakravorty, A., & Roy, S. (2024). A Review of-Photocatalysis, basic principles, processes, and materials. *Sustainable Chemistry for the Environment*, 100155.

[13] Kustiningsih, I., Pujiastuti, H., Sari, D. K., Rochmat, A., & Slamet. (2023). The addition of anthocyanin as a sensitizer for TiO2 nanotubes in a combined process of electrocoagulation and photocatalysis for methylene blue removal. *Sustainability*, **15**(21), 15384.

[14] Stewart, S., Wei, Q., & Sun, Y. (2021). Surface chemistry of quantum-sized metal nanoparticles under light illumination. *Chemical Science*, **12**(4), 1227–1239.

[15] Kanwal, H., Tahir, H., Shah, A. R., Ahmed, W., & Arsalan, M. (2023). The synthesis of titania nanoparticles (TiO2) and its methylene blue dye removal efficiency through photocatalysis based on response surface methodology (RSM). *Global Nest J*, **25**(2), 67–74.

[16] Alamier, W. M., Hasan, N., Ali, S. K., & Oteef, M. D. (2022). Biosynthesis of Ag nanoparticles using Caralluma acutangula extract and its catalytic functionality towards degradation of hazardous dye pollutants. *Crystals*, **12**(8), 1069.
[17] Zuhrotun, A., Oktaviani, D. J., & Hasanah, A. N. (2023). Biosynthesis of gold and silver nanoparticles using phytochemical compounds. *Molecules*, **28**(7), 3240.
[18] Amin, Z. S., Afzal, M., Ahmad, J., Ahmed, N., Zeshan, B., Hashim, N. H. H. N., & Yean, C. Y. (2023). Synthesis, characterization and biological activities of zinc oxide nanoparticles derived from secondary metabolites of Lentinula edodes. *Molecules*, **28**(8), 3532.
[19] Rahman, F., Majed Patwary, M. A., Bakar Siddique, M. A., Bashar, M. S., Haque, M. A., Akter, B., Rashid, R., Haque, M. A., & Royhan Uddin, A. K. M. (2022). Green synthesis of zinc oxide nanoparticles using Cocos nucifera leaf extract: characterization, antimicrobial, antioxidant and photocatalytic activity. *Royal Society Open Science*, **9**(11), 220858.
[20] Apriani, E. F., Mardiyanto, M., & Hendrawan, A. (2022). Optimization of green synthesis of silver nanoparticles from *Areca catechu L.* seed extract with variations of silver nitrate and extract concentrations using simplex lattice design method. *Farmacia*, **70**(5).
[21] Haji, B. S., & Barzinjy, A. A. (2022). Citrullus colocynthis fruit extract mediated green synthesis of silver nanoparticles: the impact of pH, temperature, and silver nitrate concentration. *e-Journal of Surface Science and Nanotechnology*, **21**(1), 61–71.
[22] Essawy, A. A. (2018). Silver imprinted zinc oxide nanoparticles: Green synthetic approach, characterization and efficient sunlight-induced photocatalytic water detoxification. *Journal of Cleaner Production*, **183**, 1011–1020.
[23] Aminuzzaman, M., Ng, P. S., Goh, W. S., Ogawa, S., & Watanabe, A. (2019). Value-adding to dragon fruit (Hylocereus polyrhizus) peel biowaste: green synthesis of ZnO nanoparticles and their characterization. *Inorganic and Nano-Metal Chemistry*, **49**(11), 401–411.
[24] Aydin Acar, C., Gencer, M. A., Pehlivanoglu, S., Yesilot, S., & Donmez, S. (2024). Green and eco-friendly biosynthesis of zinc oxide nanoparticles using Calendula officinalis flower extract: Wound healing potential and antioxidant activity. *International Wound Journal*, **21**(1), e14413.
[25] Yang, N. Q., Li, J., Wang, Y. N., & Ma, J. (2021). Investigation of photocatalytic properties based on Fe and Ce Co-doped ZnO via hydrothermal method and first principles. *Materials Science in Semiconductor Processing*, **131**, 105835.
[26] Lemecho, B. A., Sabir, F. K., Andoshe, D. M., Gultom, N. S., Kuo, D. H., Chen, X., Mulugeta, E., Desissa, T. D., & Zelekew, O. A. (2022). Biogenic synthesis of Cu-Doped ZnO photocatalyst for the removal of organic dye. *Bioinorganic Chemistry and Applications*, **2022**(1), 8081494.
[27] Amarasinghe, L. D., Wickramarachchi, P. A. S. R., Aberathna, A. A. A. U., Sithara, W. S., & De Silva, C. R. (2020). Comparative study on larvicidal activity of green synthesized silver nanoparticles and Annona glabra (Annonaceae) aqueous extract to control Aedes aegypti and Aedes albopictus (Diptera: Culicidae). *Heliyon*, **6**(6).
[28] Kemala, P., Idroes, R., Khairan, K., Ramli, M., Ginting, B., Helwani, Z., Aulia, R., Idroes, G. M., Muhammad, Y. Y., & Efendi, R. (2025). Eco-friendly synthesis of silver nanoparticles: Enhancing optimization reaction, characterization, and antimicrobial properties with Lantana camara from geothermal area. *South African Journal of Chemical Engineering*, **51**(1), 57–67.
[29] Roddu, A. K., Wahab, A. W., Ahmad, A., & Taba, P. (2019). Green-route synthesis and characterization of the silver nanoparticles resulted by bio-reduction process. *Journal of Physics: Conference Series*, 1341(3), 032004.
[30] Adam, R. E., Alnoor, H., Pozina, G., Liu, X., Willander, M., & Nur, O. (2020). Synthesis of Mg-doped ZnO NPs via a chemical low-temperature method and investigation of the efficient photocatalytic activity for the degradation of dyes under solar light. *Solid State Sciences*, **99**, 106053.
[31] Yin, X., Liu, L., & Ai, F. (2021). Enhanced photocatalytic degradation of methylene blue by WO3 nanoparticles under NIR light irradiation. *Frontiers in Chemistry*, **9**, 683765.
[32] Sundrarajan, M., Ambika, S., & Bharathi, K. (2015). Plant-extract mediated synthesis of ZnO nanoparticles using Pongamia pinnata and their activity against pathogenic bacteria. *Advanced Powder Technology*, **26**(5), 1294–1299.

[33] Cai, M., Shui, A., Wang, X., He, C., Qian, J., & Du, B. (2020). A facile fabrication and high-performance electromagnetic microwave absorption of ZnO nanoparticles. *Journal of Alloys and Compounds*, **842**, 155638.

[34] Abdelghani, G. M., Ahmed, A. B., & Al-Zubaidi, A. B. (2022). Synthesis, characterization, and the influence of energy of irradiation on optical properties of ZnO nanostructures. *Scientific Reports*, **12**(1), 20016.

[35] Khan, S., Noor, T., Iqbal, N., & Yaqoob, L. (2024). Photocatalytic dye degradation from textile wastewater: a review. *ACS Omega*, **9**(20), 21751–21767.

[36] Dewi, R., Hamzah, Y., Manik, Y., Ziliwu, F., Simbolon, N. I., Syajali, H., Maulidya, S., Ningrum, Y., & Fatanah, H. (2024). Properties of $BaTiO_3$ nanoparticles based on FTIR derived using *Nephelium lappaceum L.* leaf extract. *Science, Technology and Communication Journal*, **4**(3), 93–96.